

<sup>1</sup>Laboratory of Atmospheric Physics, Aristotle University of Thessaloniki, Greece

<sup>2</sup>Department of Earth Sciences, Hydrology, University of Uppsala, Sweden

<sup>3</sup>Agricultural University Wageningen, The Netherlands

<sup>4</sup>Wind Energy and Atmospheric Physics Department, Risø National Laboratory, Roskilde, Denmark

## Numerical model simulations of boundary-layer dynamics during winter conditions

D. Melas<sup>1</sup>, T. Persson<sup>1,2</sup>, H. De Bruin<sup>3</sup>, S.-E. Gryning<sup>4</sup>, E. Batchvarova<sup>4</sup>, and C. Zerefos<sup>1</sup>

With 7 Figures

Received November 12, 1999

Revised October 4, 2000

### Summary

A mesoscale numerical model, incorporating a land-surface scheme based on Deardorff's approach, is used to study the diurnal variation of the boundary layer structure and surface fluxes during four consecutive days with air temperatures well below zero, snow covered ground and changing synoptic forcing. Model results are evaluated against in-situ measurements performed during the WINTEX field campaign held in Sodankylä, Northern Finland in March 1997. The results show that the land-surface parameterization employed in the mesoscale model is not able to reproduce the magnitude of the daytime sensible heat fluxes and especially the pronounced maximum observed in the afternoon. Additional model simulations indicate that this drawback is to a large extent removed by the implementation of a shading factor in the original Deardorff scheme. The shading factor, as discussed in Gryning et al. (2001), accounts for the fact that in areas with sparse vegetation and low solar angles, both typical for the northern boreal forests in wintertime, absorption of direct solar radiation is due to an apparent vegetation cover which is much greater than the actual one (defined as the portion of the ground covered by vegetation projected vertically). Moreover, the observed asymmetry in the diurnal variation of the sensible heat flux indicates that there might be a significant heat storage in the vegetation. The implementation of an objective heat storage scheme in the mesoscale model explains part of the observed diurnal variation of the sensible heat flux.

### 1. Introduction

The ability of General Circulation Models to simulate climate and to predict climate change is strongly dependent on an adequate representation of processes at the soil-vegetation-atmosphere interface. A better understanding of these key components in the climate system at different scales might lead to an improvement of climate change simulations. Present scenarios stress that changes in wintertime temperature at high latitudes may have a large impact on climate change (Houghton et al., 1996). The role of the northern hemisphere boreal forest zone in the climate system and the interaction between snow-covered ground, vegetation and atmosphere has been investigated in a number of studies which have highlighted the need for more realistic parameterizations for snow-vegetation systems in climate models (Thomas and Rowntree, 1992; Douville et al., 1995; Essery, 1998). Large scale model studies have addressed the large climatic effects of increasing surface albedo due to deforesting and increased snow cover on the northern hemisphere (Thomas and Rowntree, 1992; Douville and Royer, 1997).

Stand-alone experiments performed by Douville and Royer (1997) shows that the atmospheric boundary-layer can be heated by the forest even when the ground is snow covered. Harding and Pomeroy (1996) show a strong modification of the energy balance in a boreal forest depending on whether there is intercepted snow on the forest canopy or not. Essery (1997) uses a boundary layer model to simulate and compare fluxes from surfaces with heterogeneous snow cover and snow-free vegetation addressing the difficulties of calculating effective parameters for regions with both upward and downward heat fluxes which can occur when a heterogeneous snow-cover is present.

Current land-surface parameterization schemes used in larger scale models have mainly been developed and tested for conditions prevailing during the warm part of the year since most of the large-scale climate experiments used for validation of the schemes have been carried out during summer seasons, e.g. HAPEX-MOBILHY (André et al., 1986) and FIFE (Sellers et al., 1992). Recently, experiments have taken place in the northern hemisphere boreal forests including measurements performed during winter conditions, e.g. BOREAS (Sellers et al., 1997), NOPEX (Halldin et al., 1998) with the winter field campaign WINTEX (Harding et al., 1999). These climate experiments have provided data with good temporal and spatial coverage to test and adapt land-surface parameterizations used in large scale models for winter conditions.

The boreal forest covers large areas of Scandinavia, Canada, and Russia. The boreal forest zone is dominated by coniferous trees and the canopies are often very sparse. One of the most striking features of the boreal forest zone is that the ground (but not necessarily the vegetation) is covered with snow for a large part of the year. The snow surface has a very high reflectivity for short-wave radiation; the albedo can reach 90%, thus reducing the net radiation. With its low heat conductivity, the snow acts as a thermal insulator between soil and vegetation. Flux measurements with fast response instruments during WINTEX reveal that in a sparse forest with snow-covered ground and temperatures well below zero the sensible heat fluxes can occasionally exceed  $130 \text{ W/m}^2$  (Batchvarova et al., 2001; Gryning et al., 2001).

In the present study a mesoscale model with the widely used land-surface parameterization presented by Deardorff (1978) is tested against in-situ measurements performed during WINTEX in March 1997. The model concept presented by Deardorff (1978) has been the base for many parameterizations of different degrees of complexity such as BATS (Dickinson et al., 1986), SiB (Sellers et al., 1986) and ISBA (Noilhan and Planton, 1989) among others. In the Deardorff formulation the canopy is treated as a bulk layer, with its own temperature, separated from the snow-covered ground. The canopy energy balance is solved instantly, i.e. it is assumed that there is no heat storage in the vegetation. The vegetation cover is represented by a fraction,  $\sigma_f$ .

Based on a comparison between the in-situ measurements and simulations, two simple modifications are implemented in the present scheme to explore effects not satisfactorily simulated by the original Deardorff scheme; *i*) A shading factor together with a transmittancy factor to compensate for the apparent high vegetation cover due to low solar angles (Gryning et al., 2001); *ii*) A simple heat storage expression to compensate for the asymmetry in the simulated daytime sensible heat fluxes (Grimmond et al., 1991).

## 2. The experiment, area and the observations

Between March 12 and April 19, 1997, an experimental campaign took place within WINTEX. The campaign included aircraft measurements, remote-sensing and a network of micro-meteorological field stations at the southern and northern WINTEX sites located around Uppsala, central Sweden and Sodankylä, northern Finland, respectively. In the present study data from Sodankylä in the northern WINTEX region has been used.

The Sodankylä Meteorological Observatory (SMO) is located in a sub-arctic forest area in northern Finland (67,29 N; 26,39 E; 179 m AMSL; central Lapland) and operated by the Finnish Meteorological Institute. The terrain around SMO is moderately undulating with isolated hills reaching up to 500 m altitude (Fig. 1). The region surrounding SMO ( $100 \times 100 \text{ km}^2$ ) is dominated by coniferous forest (36%) with pine as the most abundant species. Mixed/deciduous forest

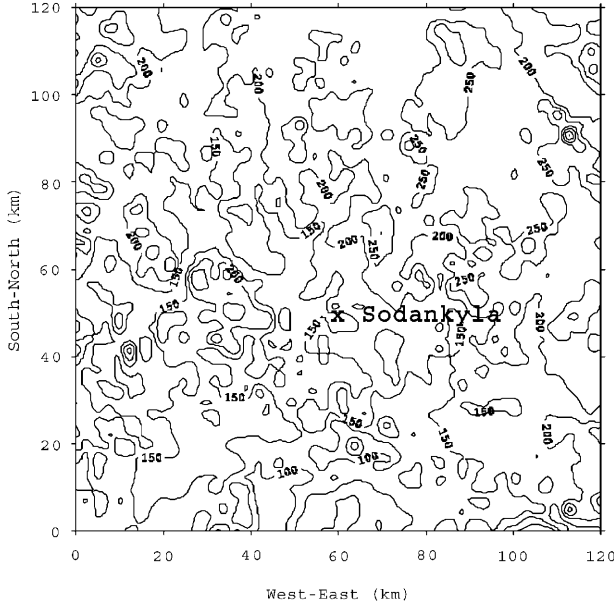


**Fig. 1.** Map of WINTEX region where the Sodankylä measuring site is indicated. Height contours in meters

accounts for 13% of the land cover. Peatbogs that include open peatlands, and sparsely vegetated peatlands has a coverage of 23%. Classified as “transitional woodland shrub” including conifer plantations and clear cuttings also accounts for 23%. Lakes and rivers cover roughly 3% of the region.

For the WINTEX campaign a 18 m high mast was erected in a sparse coniferous forest at SMO with a typical tree height of 7–9 m. During the studied period the trees were free from snow. Eddy-correlation measurements performed with Solent Research 3D sonic anemometers at a frequency of 10 Hz were used in this study. The measurements were performed in and above the sparse forest at heights 2, 6, 12 and 18 m. Details about the experimental setup and the collected data are given in Halldin (1999) and Gryning et al. (2001). Moreover, during the WINTEX campaign, radio-soundings were performed at SMO with three hours interval. As part of the standard synoptic observation programme, hourly observations of cloud cover were carried out (Halldin, 1999).

Information of the vegetation cover was obtained from a digitized landuse map with a resolution of 1 km. The topographical information was derived from a Digital Elevation Model with a horizontal resolution of 1 km.

### 3. Model formulation

#### 3.1 Mesoscale model

The mesoscale model used in the present study is developed at the Meteorological Institute at Uppsala University (MIUU) and is well documented in the literature (Enger, 1990; Tjernström, 1987). Only a brief summary will be presented in this section.

A terrain influenced coordinate system is used to introduce the topography in the model. The new vertical coordinate,  $\eta$ , is defined as

$$\eta = s \frac{z - z_g}{s - z_g} \quad (1)$$

where  $s$  is the height of the model top, constant in this study,  $z$ , is the actual height Above Mean Sea Level (AMSL) and,  $z_g$ , is the terrain height.

All model equations are transformed into the new coordinate system. The pressure terms in the transformed equations have been decomposed into two parts. The large scale pressure force is expressed with the geostrophic wind, and the other two pressure terms in the equations represent the mesoscale forcing. Given the condition that the terrain slope is much less than  $45^\circ$ , the pressure field is determined according to Pielke and Martin (1981).

The turbulent exchange coefficients in this model are determined in terms of the turbulent kinetic energy, obtained from a prognostic equation. The turbulence closure is based on the approach developed by Yamada and Mellor (1975), the ‘Level 2.5’ model (distinguishing it from ‘Level 3’ which also includes a prognostic equation for potential temperature variance). The remaining turbulent moments are determined by diagnostic expressions. Details of the parameterization of higher order terms are found elsewhere (Launder et al., 1975; Lumley, 1979; Mellor, 1973; Andrén, 1990). The turbulent exchange coefficient for momentum is given in the MIUU-model by:

$$K_M = A_1 \lambda q^3 \left[ (1 - 3c)q^2 + 3A_2 \lambda^2 \{ (B_2(1 - \alpha_2) - 3A_2) - 3c(4A_1 + B_2(1 - \alpha_2)) \} \beta g \frac{\partial \Theta}{\partial z} \right] \\ \div q^4 + 6A_1^2 \lambda^2 q^2 \left| \frac{\partial \mathbf{V}}{\partial z} \right|^2 + 3A_1 A_2 \lambda^2 \beta g \frac{\partial \Theta}{\partial z}$$

$$\begin{aligned} & \times \left\{ 6A_1\lambda^2(B_2(1 - \alpha_2) - 3A_2) \left| \frac{\partial V}{\partial z} \right|^2 \right. \\ & + (7 + B_2(1 - \alpha_2)/A_1)q^2 + 9A_2\lambda^2 \\ & \left. \times (4A_1 + B_2(1 - \alpha_2))\beta g \frac{\partial \Theta}{\partial z} \right\} \quad (2) \end{aligned}$$

and the turbulent exchange coefficient for heat is given by:

$$\begin{aligned} K_H &= A_2\lambda \left[ q^3 - 6A_1\lambda K_M \left| \frac{\partial \mathbf{V}}{\partial z} \right|^2 \right] \\ & \div \left[ q^2 + 3A_2\lambda^2(4A_1 + B_2(1 - \alpha_2))\beta g \frac{\partial \Theta}{\partial z} \right] \quad (3) \end{aligned}$$

where

$$\left| \frac{\partial \mathbf{V}}{\partial z} \right|^2 = \left( \frac{\partial U}{\partial z} \right)^2 + \left( \frac{\partial V}{\partial z} \right)^2 \quad (4)$$

and  $q^2$  is double the turbulent energy;  $\beta$  is a coefficient of thermal expansion;  $g$  is the acceleration of gravity;  $\Theta$  is the mean potential temperature;  $U$  and  $V$  are the mean wind speed in  $x$ - and  $y$ -directions, respectively;  $A_1, A_2, B_1, B_2, c$  and  $\alpha_2$  are empirical constants. Details about the turbulent length scale,  $\lambda$ , can be found in Enger (1990).

The advection scheme used in the model has been corrected for numerical diffusion and is of third order both in time and space. Zero gradient inflow – gradient outflow is used for the lateral boundary conditions (Tjernström et al., 1988). The gradient at the inflow boundary is equal to zero while air exiting the model is assumed to have the same value as found one grid point upstream. Due to the telescoping grid used in the present model, the lateral boundaries are located far enough from the region of interest to reduce the influence of the lateral boundary errors propagating into the area of interest. At four grid points at the lateral boundaries a “flow relaxation scheme” is applied in order to allow a temporal variation of the geostrophic wind (e.g., Davies, 1983). The scheme is successfully used in both atmosphere and ocean models (Davies, 1983; Engedahl, 1995).

### 3.2 Land-surface parameterization

The land-surface parameterization used in the MIUU model is the scheme presented by

Deardorff (1978) with some modifications that are presented in this section. Deardorff’s scheme achieves a good balance between complexity and input data requirement and is the base for several land surface schemes currently employed in meso- and large-scale models, e.g. BATS (Dickinson et al., 1986), SiB (Sellers et al., 1986) and ISBA (Noilhan and Planton, 1989). The performance of the Deardorff scheme has been compared with other land-surface parameterizations for a sparse vineyard canopy in van den Hurk et al. (1995).

The parameterization includes a canopy layer, which interacts both with the atmosphere and the underlying surface, and carries a prognostic equation for surface temperature. The parameterization also include a prognostic equation for soil moisture, but this is omitted in the present study since the ground is frozen and covered with snow to a depth of  $\sim 90$  cm. The scheme is adapted to snow conditions by simply changing the soil thermal properties to values representative for a deep snow pack.

The incoming short-wave radiation in the MIUU-model is parameterized as:

$$S^\downarrow = (t_r - a_q)S_0 \quad (5)$$

where  $t_r$  is the fractional transmissivity of short-wave irradiance at the ground that accounts for downward Rayleigh scattering and absorption of diffuse irradiance (Kondratyev, 1969);  $a_q$  is the absorption of direct irradiance (McCumber, 1980) and  $S_0$  is the direct downward solar irradiance reaching a horizontal surface of unit area at the top of the atmosphere.

The fluxes of long-wave radiation are calculated using an emissivity model following Atwater (1974), Kuhn (1963) and Kondratyev (1969). The flux of downward long-wave radiation is obtained by integrating from the top of the model down to the top of the canopy layer.

The exchange coefficient for heat and moisture transfer are assumed to be equal and are calculated by:

$$c_H = \left( \frac{u_*}{u_a} \right)^2 \quad (6)$$

where  $u_*$  is the friction velocity taken from the meso-scale model and  $u_a$  is equal to the wind at the third model level ( $\sim 9$  m AGL).

In the MIUU model each grid cell is subdivided into a vegetated part, covering a fraction  $\sigma_f$ , and a

non-vegetated part covering a fraction  $(1 - \sigma_f)$  of the grid cell surface area. The latent and sensible heat fluxes from these areas are calculated separately and the total flux to the atmosphere is obtained by a weighted sum of the fractional fluxes from the vegetated and non-vegetated surface areas respectively. The total sensible heat flux from a MIUU grid cell to the atmosphere is:

$$H_{\text{tot}} = (1 - \sigma_f)H_{sg} + \sigma_f(H_{sgf} + H_{sf}) \quad (7)$$

where subscript *sg* refers to the snow surface, *sgf* to the snow surface beneath the canopy and *sf* to the vegetation, respectively.

The total latent heat flux is:

$$E_{\text{tot}} = (1 - \sigma_f)E_{sg} + \sigma_f(E_{sgf} + E_f) \quad (8)$$

where the subscripts are the same as in Eq. (7)

It should be noted that the snow surface energy balance formulation does not include an expression for snowmelt. However, during the simulated four-day period the observed air temperatures close to the snow surface were always below 0°C.

### 3.3 Absorption of direct solar radiation by the forest

The sparse high-latitude forest is a very effective absorber of short-wave radiation. Under low solar angle conditions, a large portion of the direct solar radiation is absorbed by the canopy which is apparently covering the ground. In order to describe the effect of low solar angles which leads to an apparent high vegetation cover for direct solar radiation Gryning et al. (2001) introduce a shading factor,  $f_{sh}$ . The shading factor is generally a function of  $\sigma_f$  and the solar angle,  $\alpha$ . A simple expression for  $f_{sh}$  is derived in Gryning et al. (2001):

$$f_{sh} = \sigma_f \left( 1 + \frac{4h}{\pi d \tan \alpha} \right) \quad \alpha \geq \alpha_c \quad (9)$$

where  $h$  is the height of the trees and  $d$  is the crown diameter. The critical solar angle,  $\alpha_c$ , below which the ground is fully shaded, i.e.  $f_{sh} = 1$ , can be estimated with the expression:

$$\tan(\alpha_c) = \frac{4h}{\pi d} \left( \frac{\sigma_f}{1 - \sigma_f} \right) \quad (10)$$

Gryning et al. (2001) also introduce a transmittancy factor,  $\tau$ , describing the fact that the sparse vegetation is not opaque for solar radiation. If the

canopy is entirely transparent,  $\tau$  will be equal to unity and if the canopy is opaque,  $\tau$  will be equal to zero.

With the implementation of a shading factor and a transmittancy factor the gain of short-wave radiation for the snow cover and the vegetation canopy will be expressed differently from that proposed by Deardorff (1978). Gryning et al. (2001) divide the short-wave radiation received by the canopy into three terms. The first refers to the diffuse solar radiation which is treated as in Deardorff (1978). The second term refers to the direct solar radiation received by the canopy and the third term describes the reflected short-wave radiation received by the canopy from the snow cover. The following equation is introduced:

$$S_c^G = \sigma_f D + f_{sh}(1 - \tau)I \sin \alpha + \sigma_f a_g(1 - \tau)S_s^G \quad (11)$$

in which  $D$  is the diffuse component of the incoming short-wave radiation,  $I$  is the incoming solar radiation at the top of the vegetation across a plane perpendicular to the solar beam and  $a_g$  is the snow surface albedo. The short-wave radiation received by the snow cover is expressed as:

$$S_s^G = (1 - \sigma_f)D + f_{sh}\tau I \sin \alpha + (1 - f_{sh})I \sin \alpha \quad (12)$$

The implementation of a shading factor and a transmittancy factor will thus modify the partitioning of direct short-wave radiation between the snow surface and the vegetation and thus have a different impact on the snow surface and foliage temperatures as compared with Deardorff's scheme. Throughout the day, the shading will then effect the partial contributions to the total sensible heat flux to the atmosphere from the snow surface and the vegetation as given in Eq. (7). The maximum value of the shading factor,  $f_{sh}$ , is unity and its minimum value is equal to the shielding factor,  $\sigma_f$ . The shading factor for the studied case is equal to one for the entire day. The transmittancy factor is generally a function of the solar angle and extensive data are required for the empirical determination. As a first approximation a constant value,  $\tau = 0.3$ , is used in the present study.

### 3.4 Heat storage

The model by Deardorff assumes no heat storage in the vegetation and the energy balance of the

vegetation is solved instantly. This concept is valid in soil-vegetation systems where the ground is the major storage for heat due to its large heat capacity.

When a snow-cover with a very low heat capacity is present the ground is no longer dominant and the vegetation becomes the system's major heat source and sink. Studies have shown that the time constant for heating of trunks of trees can be up to several hours (Monteith, 1981).

In the present study an objective hysteresis model is implemented in the mesoscale model to predict the heat storage by the vegetation (Grimmond et al., 1991):

$$\Delta H_{sf} = a_1 Q^* + a_2 (\partial Q^* / \partial t) + a_3 \quad (13)$$

where  $Q^*$  is the net all-wave radiation flux density,  $a_1, a_2$  and  $a_3$  are dimensionless coefficients with the values  $a_1 = 0.11$ ,  $a_2 = 0.11 \text{ h}$  and  $a_3 = -12.3 \text{ Wm}^{-2}$  for mixed forest (McCaughy, 1985).

#### 4. Model setup and initialization

The numerical simulations in WINTeX were performed for a horizontal domain of  $120 \times 120 \text{ km}^2$  centered approximately over Sodankylä Meteorological Observatory. In the horizontal a telescoping grid is employed, the grid distance being 2.0 km in the central parts of the model and expanding towards the lateral boundaries. The total number of grid points on each vertical level is  $37 \times 37$ . In order to properly resolve the sharp surface layer gradients of meteorological parameters, vertical grid levels are log linearly spaced, with mean and turbulent quantities vertically staggered. The vertical resolution at the lower boundary is chosen to be 2 m. The vertical coordinate contains 20 levels up to the model top, which is set at 7000 m AMSL.

The simulation period extends over four days, namely 15–18 March 1997. During this period, cloud conditions were ranging from cloud-free to overcast. The input data were determined from the rawinsonde measurements at Sodankylä. The forcing at the lateral boundaries was updated every six hours. At the onset of the integration there is no topography in the model during 6 hours of integration. After this initialization period, the real simulation starts at 2.00 LST with the terrain at its assigned height. The time step is 10 s. The

cloud cover for the simulated period was prescribed according to the observations performed at the SMO.

To illustrate the impact of the implemented shading factor and heat storage scheme on the model results, three test runs have been carried out:

1. A control run with the original land-surface parameterization (section 3.2)
2. A simulation where a shading factor is implemented in the land-surface parameterization (see details in section 3.3)
3. A simulation including both a shading factor and an objective model for heat storage in the vegetation (details are given in sections 3.3 and 3.4 respectively).

#### 5. Results and discussion

Before proceeding to the presentation of the results for the surface fluxes it is important to assess the accuracy of the calculated solar radiation. For this purpose, a comparison was made between model predictions and existing observations of the global radiation. The comparison results revealed a very good agreement as the correlation between predicted and observed values was 0.98 the bias was  $-3.8 \text{ Wm}^{-2}$  and the root mean square of error was  $26.4 \text{ Wm}^{-2}$ .

The simulation results for the four-day period are presented in comparison to existing observations in Figs. 2–4. The diurnal cycles of the sensible and latent heat fluxes and the friction velocity are depicted in Fig. 2. During the entire period, the latent heat flux exhibits a very small variation, being close to zero during nighttime and reaching a maximum of  $20\text{--}30 \text{ Wm}^{-2}$  at afternoon hours (Fig. 2a). During the last two days (17–18 March) the observations indicate a sharp maximum of  $\sim 50 \text{ Wm}^{-2}$  in morning hours. The relatively small values of latent heat fluxes are attributed to the low temperatures and the associated high stomatal resistance (Table 1). The simulation results of the three model runs are almost identical, being in close agreement with the observations, except for the morning maximum which is not reproduced by the model.

In contrast to the latent heat fluxes, the sensible heat fluxes show a remarkable diurnal variation (Fig. 2b). At night, the sensible heat fluxes at the

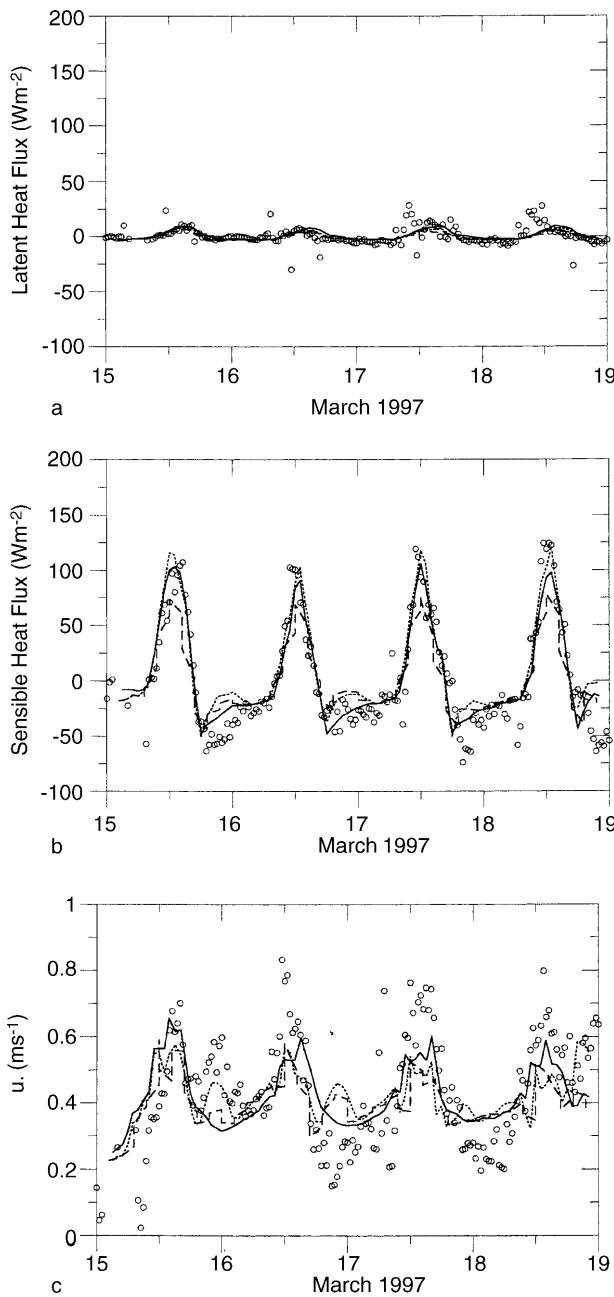


**Fig. 2.** The variation of latent heat flux (a), sensible heat flux (b) and friction velocity (c) at Sodankylä site during the period 15–18 March 1997. Circles: Observations at 12 m AGL (latent heat flux at 18 m AGL); Dashed line: Control simulation; Dotted line: Simulation results with the MIUU model implementing a shading factor; Full line: Simulation results with the MIUU model implementing a shading factor and heat storage in vegetation

Sodankylä site have small-to-moderate negative values. Approximately two hours after sunrise, the sensible heat flux becomes positive and, subsequently, steadily increases reaching approximately  $\sim 100 \text{ Wm}^{-2}$  at midday. Most of the days the

**Table 1.** Parameters in the land surface scheme

$a_g$	Albedo for snow	0.8
$a_f$	Albedo for coniferous forest	0.1
$\varepsilon_s$	Emissivity for snow surface	0.95
$\varepsilon_f$	Emissivity for coniferous forest	0.95
$z_{0s}$	Roughness length for snow	0.001 m
$z_{0f}$	Roughness length for coniferous forest	1.5 m
$\sigma_f$	Shielding factor for less dense coniferous forest	0.5
$r_{s_{\min}}$	Minimum stomatal resistance	2000 s/m
$h_{tr}$	Height of the trees	8 m
$r_{tr}$	Crown radius of the trees	2.5 m

sensible heat flux shows a “tail” of relatively high values into the late afternoon, a feature which is typical of the diurnal cycle of the surface heat flux over urban areas (Oke, 1987). This feature is more pronounced during the 15<sup>th</sup> of March which was a clear day. During the same day, the sensible heat flux exhibits a sharp maximum at  $\sim 15.00$  LST. The original energy balance scheme implemented in the MIUU model is unable to reproduce the magnitude of the observed sensible fluxes, especially at midday. The underestimation of the observed maximum is  $30\text{--}40 \text{ Wm}^{-2}$ . The implementation of the shading factor in the surface energy balance improves the agreement of the simulation results with the observations (Fig. 2b). The maximum fluxes are still underestimated but only by  $\sim 10 \text{ Wm}^{-2}$ . The inclusion of the objective heat storage scheme explains parts of the diurnal variation of the sensible heat fluxes, but there are still some discrepancies. This addresses the need to evaluate the coefficients  $a_1$  to  $a_3$  used in Eq. (13) for a sparse sub-arctic forest.

The observed friction velocities show large variations both during the diurnal cycle as well as at much shorter time scales. The simulated fluctuations are less pronounced than the observed ones and it seems that the model produces smoother variations. An interesting feature is the secondary maximum of the friction velocity observed during the night between the 15<sup>th</sup> and the 16<sup>th</sup> March, which might have been caused by katabatic flow developing during nighttime. As expected, the control run underestimates the observed friction velocities.

The near surface temperature exhibits a remarkable diurnal variation (Fig. 3), the daily range being  $\sim 20^\circ\text{C}$ . As expected, the results of the

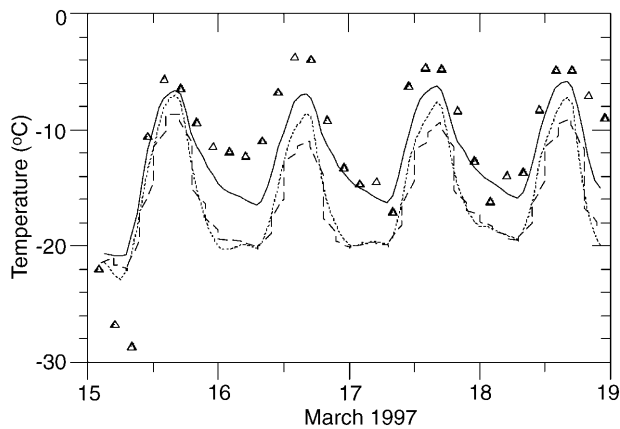


**Fig. 3.** The variation of temperature at Sodankylä site during the period 15–18 March 1997. Triangles: SYNOP measurements; Dashed line: Control simulation; Dotted line: Simulation results with the MIUU model implementing a shading factor; Full line: Simulation results with the MIUU model implementing a shading factor and heat storage in vegetation

control run underestimate the maximum temperature values observed during afternoon hours. The implementation of the shading factor improves the agreement between model simulations and observations but the observed maximum temperatures are still underestimated by a few °C. Finally, the impact of the heat storage is significant and it improves the ability of the model to reproduce the observed diurnal variation of temperatures. This is a step in the right direction but the observations indicate a stronger effect.

Besides the surface temperature, the surface fluxes strongly depend on the temperature difference between the surface and the atmospheric reference level. An error in the simulated temperature at the atmospheric reference level will effect on the error in the surface temperature. A comparison of the differences in observed temperature between 2 and 18 m and the differences in simulated temperature between the surface and the third model level at (9 m AGL) is shown in Fig. 4. There is a fairly good agreement between the observed and simulated differences. However, the mesoscale model underestimates the temperature difference at midday, which have an impact on the calculated surface fluxes.

Figure 5 shows the diurnal variation of the surface wind speed and direction. It is seen that in addition to the diurnal cycle, there is a trend during the simulated period. The winds are slightly

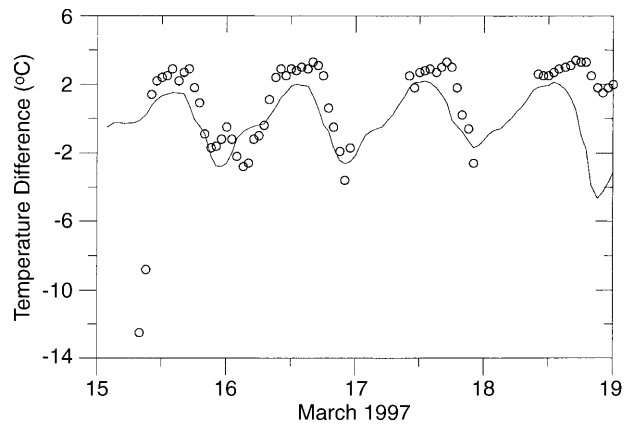


**Fig. 4.** Comparison between observed and simulated temperature differences at Sodankylä site during the period 15–18 March 1997. Circles: The difference between observed temperature at 2 and 18 m ( $T_{\text{obs}2\text{m}} - T_{\text{obs}18\text{m}}$ ). Full line: Simulated difference between the surface and the 3rd model level ( $T_{\text{modsurf}} - T_{\text{mod}9\text{m}}$ )

increasing, turning from NW to N-NNE. The results from model run 3 show a fairly good agreement with observations, while the control run seriously underestimates the observed wind speeds at daytime. This indicates the profound influence of stability on the near surface winds.

In order to further investigate the boundary layer dynamics in the area some plots are presented for the first day of the simulation period, namely the 15<sup>th</sup> March 1997. The simulated near surface ( $\sim 9$  m AGL) wind fields are shown in Fig. 6a-b at the two hours, 5.00 and 15.00 LST, when the conditions are considered to be representative of nighttime and daytime conditions. Only the simulation results from the model version including a shading factor and a heat storage scheme (test run 3) are shown here. Thermo-topographic effects dominate nighttime patterns of the low-level winds. The model results show that due to the prevailing stability the near surface winds are rather weak and variable (Fig. 6a). The most notable feature of the flow field is the development of katabatic winds, which are shown to prevail over the slopes of the hills. This is rather surprising as the topography in the area is rather gentle. The downslope flow can occasionally exceed  $4 \text{ ms}^{-1}$ . However, this is a very shallow system as the wind field at  $\sim 72$  m AGL (not shown here) does not show the same influence. The daytime near-surface wind pattern is

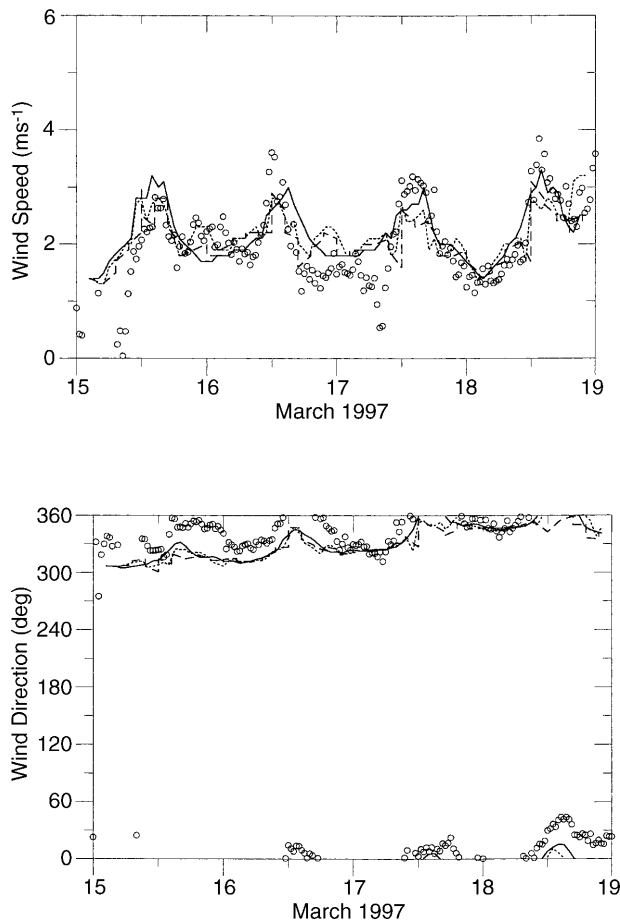


**Fig. 5.** Diurnal variation of the near surface wind speed (a) and direction (b). Circles: Observations with the sonic anemometer at 12 m AGL; Dashed line: Control simulation; Dotted line: Simulation results with the MIUU model implementing a shading factor; Full line: Simulation results with the MIUU model implementing a shading factor and a scheme for heat storage in vegetation

dominated by northwesterly flow of weak-to-moderate intensity (Fig. 6b). The wind field is rather homogenous with only a few significant features. This is attributed to the gentle topography of the area, which during daytime has only a minor impact on the flow.

The development of the daytime boundary layer is shown in Fig. 7a-c which depict the diurnal variation of the potential temperature profiles for the three model runs during the 15<sup>th</sup> March. All three runs indicate the existence of an unstable layer which starts developing during morning hours. However, there are distinct differences in both the time when the burning off of the nocturnal inversion starts and the depth of the

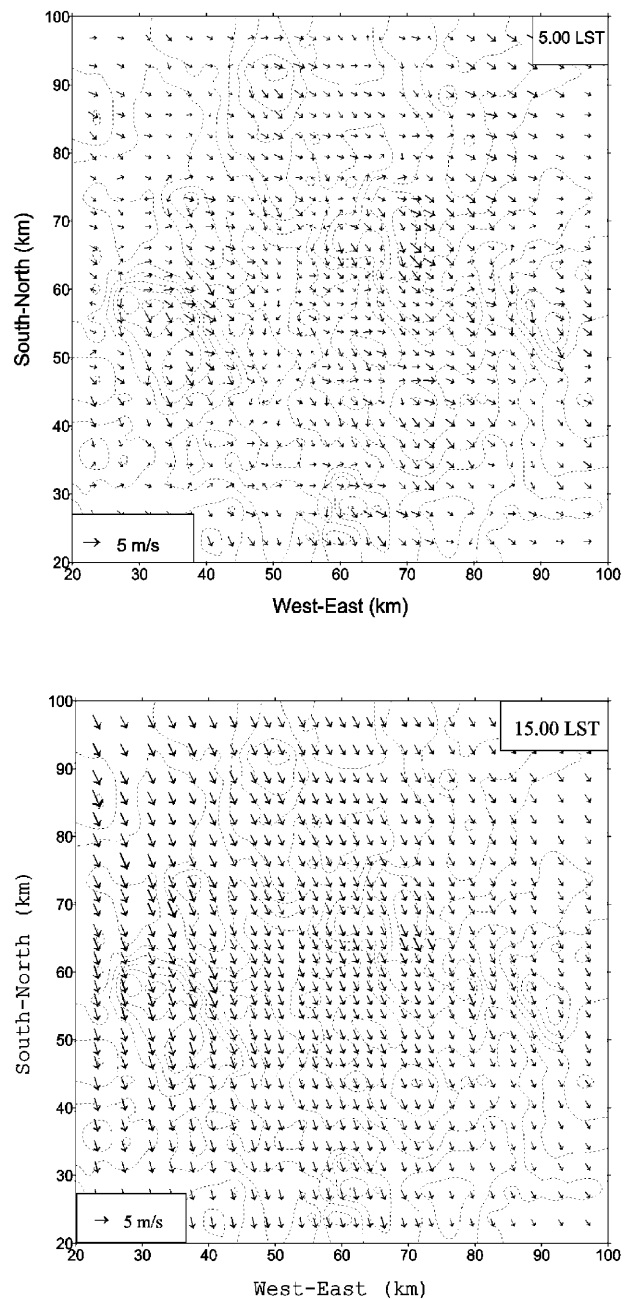


**Fig. 6.** Simulated near surface wind field at the 15<sup>th</sup> March 1997 at (a) 5.00 LST and (b) 15.00 LST. Dashed lines are terrain heights

unstable layer. As expected, the control run, which seriously underestimates the surface turbulent fluxes, predicts a very shallow unstable layer which starts developing approximately one hour later (Fig. 7a). On the other hand, the differences between test runs 2 and 3 are very small, being restricted to evening and night hours, when the model version including a heat storage scheme

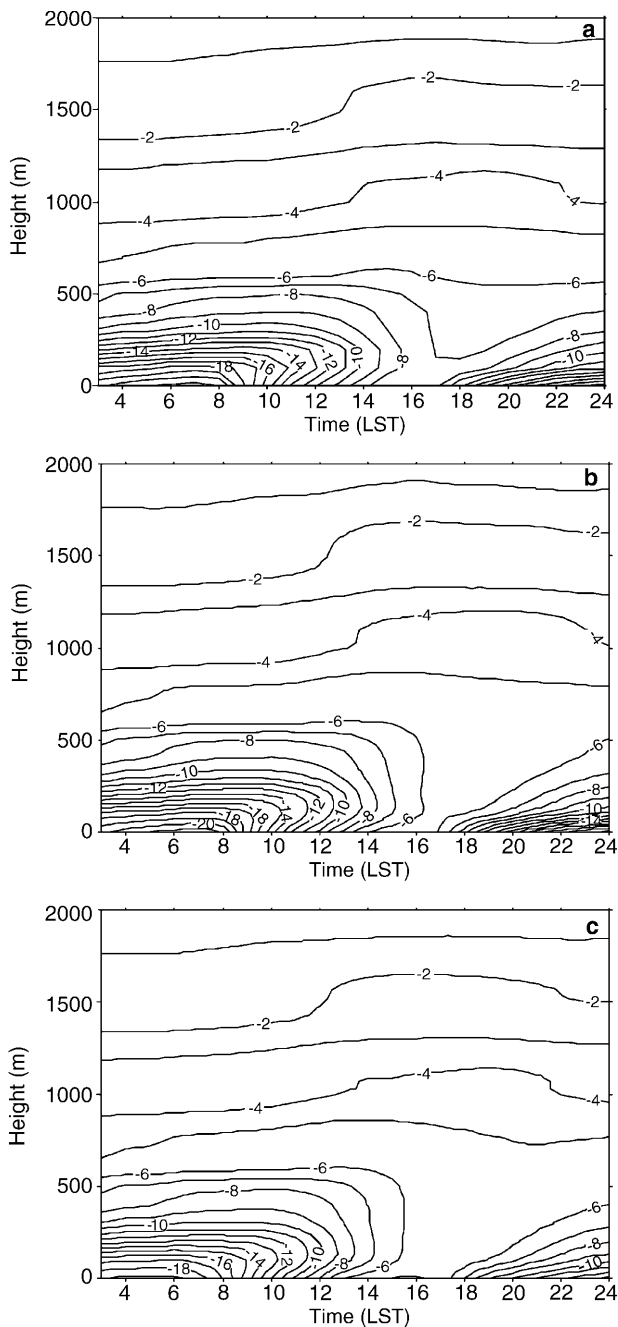


**Fig. 7.** A plot comparing the simulated diurnal variation of potential temperature profiles at the 15<sup>th</sup> March 1997 at Sodankylä site; (a) control simulation; (b) simulation with the model implementing a shading factor; (c) simulation with the model implementing a shading factor and the heat storage model

predicts higher temperatures and a slower evolution of the nocturnal inversion. The maximum height of the unstable layer is  $\sim 600$  m and is predicted to occur at  $\sim 16.30$  LST.

## 6. Summary and conclusions

The three-dimensional, higher order turbulence closure model, MIUU, was used to simulate the surface turbulent fluxes, the winds and the boundary layer structure over a sparse forest during wintertime conditions. Numerical simulation results were compared with existing observations from the WINTEX campaign, which was carried out in March 1997. A four days period with a remarkable diurnal range of temperature was chosen for simulation, March 15–18, 1997.

The existing surface energy balance scheme, based on Deardorff (1978), was found to underestimate the high values of sensible heat flux observed at midday and afternoon hours. Consequently, all other boundary layer parameters that are related to the prevailing stability conditions (temperature, wind speed, friction velocity, and to less extend wind direction) are affected accordingly. In order to remove this discrepancy, two simple modifications are implemented in the model *i*) A shading factor together with a transmittancy factor to compensate for the apparent high vegetation cover due to low solar angles (Gryning et al., 2001); *ii*) A simple expression for heat storage in the canopy to compensate for the asymmetry in the simulated daytime sensible heat fluxes and temperatures (Grimmond et al., 1991). It is found that the inclusion of the shading factor and the transmittancy factor in the surface energy balance scheme produces sensible heat fluxes during daytime which are in good agreement with the observed ones. The impact of the expression for the heat storage in vegetation in the results is smaller and it indicates the need to evaluate the coefficients used for a sparse high latitude forest.

## Acknowledgements

This work was supported by the European Commission under the contracts ENV4-CT96-0324 (Melas) and ERB4001GT980674 (Persson).

## References

- André J-C, Goutorbe J-P, Perrier A (1986) HAPEX-MOBILHY: a hydrologic atmospheric experiment for the study of water budget and evaporation flux at the climatic scale. *Bull Amer Meteor Soc* 67: 138–144
- Andrén A (1990) Evaluation of a turbulence closure scheme suitable for air-pollution applications. *J Appl Meteor* 29: 224–239

- Atwater MA (1974) The radiation model, Sect 1, Vol 1, CEM Rep No 5131-4099. In: A description of a general three-dimensional numerical simulation model of a coupled air-water and/or air-land boundary layer. Hartford, Connecticut: Centre for the Environment and Man, pp 67–82
- Batchvarova E, Gryning S-E, De Bruin H (2000) Parameterisation of fluxes over a sparse boreal forest at high latitudes. In: Gryning S-E, Schiermeier F (eds) Air pollution modeling and its application, Vol XIV. New York: Kluwer Academic/Plenum Press, pp 427–435
- Davies HC (1983) Limitations of some common lateral boundary schemes used in regional NWP models. *Mon Wea Rev* 111: 1002–1012
- Deardorff JW (1978) Efficient prediction of ground surface temperature and moisture, with inclusion of a layer of vegetation. *J Geophys Res C* 83: 1889–1903
- Dickinson RE, Henderson-Sellers A, Kennedy PJ, Wilson MF (1986) Biosphere-Atmosphere Transfer Scheme (BATS) for the NCAR community climate model. NCAR Technical Note NCAR/TN-275+STR. Boulder, Colorado: National Center for Atmospheric Research, 69 pp
- Douville H, Royer J-F, Mahfouf J-F (1995) A new snow parameterization for the Meteo-France climate model. Part I: validation in stand-alone experiments. *Clim Dyn* 12: 21–35
- Douville H, Royer J-F (1997) Influence of the temperate and boreal forests on the Northern Hemisphere climate in the Meteo-France climate model. *Clim Dyn* 13: 57–74
- Enegdahl H (1995) Use of the flow relaxation scheme in a three dimensional baroclinic ocean model with realistic topography. *Tellus* 47A: 365–382
- Enger L (1990) Simulation of dispersion in moderately complex terrain. Part A: The fluid dynamic model. *Atmos Environ* 24: 2431–2446
- Essery R (1997) Modelling fluxes of momentum, sensible heat and latent heat over heterogeneous snow cover. *Quart J Roy Meteor Soc* 123: 1867–1883
- Essery R (1998) Boreal forests and snow in climate models. *Hydrol Process* 12: 1561–1567
- Grimmond CSB, Cleugh HA, Oke TR (1991) An objective urban heat storage model and its comparison with other schemes. *Atmos Environ* 25B: 311–326
- Gryning S-E, Batchvarova E, De Bruin H (2001) The energy balance for a sparse coniferous high-latitude forest under winter conditions. *Bound-Layer Meteor* 99: 465–488
- Halldin S (1999) Final report for WINTEX. Technical Report No 29. Uppsala: NOPEX Central Office, Uppsala University, 70 pp
- Halldin S, Gottschalk L, van de Griend AA, Gryning S-E, Heikinheimo M, Högrström U, Jochum A, Lundin L-C (1998) NOPEX – A Northern hemisphere climate processes land-surface experiment. *J Hydrol* 212–213: 172–187
- Harding R, Gryning S-E, Halldin S, Lloyd C (2001) Progress in understanding of land/atmosphere exchanges at high latitudes. *Theor Appl Climatol* 70: 5–18
- Harding R, Pomeroy J (1996) The energy balance of the winter boreal landscape. *J Climate* 9: 2778–2787
- Houghton JT, Meira Filho LG, Calander BA, Harris N, Kattenberg A, Varney SK (eds) (1996) *Climate Change 1995. The Science of Climate Change*. Cambridge: University Press, 572 pp
- Kondratyev KA (1969) *Radiation in the atmosphere*. International Geophysics Series. New York: Academic Press
- Kuhn P (1963) Radiometer observations of infrared flux emissivity of water vapour. *J Appl Meteor* 2: 368–378
- Lauder G, Reece J, Rodi W (1975) Progress in the development of a Reynolds stress turbulent closure. *J Fluid Mech* 68: 537–566
- Lumley JL (1979) Computational modeling of turbulent flows. *Adv Appl Sci* 18: 123–176
- McCaughey JH (1985) Energy balance storage terms in a mature mixed forest at Petawawa Ontario – a case study. *Bound-Layer Meteor* 31: 89–101
- McCumber MC (1980) A numerical simulation of the influence of heat and moisture fluxes upon mesoscale circulations. PhD Dissertation. Charlottesville: University of Virginia, 255 pp
- Mellor GL (1973) Analytic prediction of the properties of stratified planetary surface layers. *J Atmos Sci* 30: 1061–1069
- Monteith JL (1981) Coupling of plants to the atmosphere. In: Grace J, Ford ED, Jarvis PG (eds) *Plants and their atmospheric environment*. Oxford: Blackwell Scientific Publications, pp 1–29
- Noilhan J, Planton S (1989) A simple parameterization of land surface processes for meteorological models. *Mon Wea Rev* 117: 536–549
- Oke TR (1987) The surface energy budgets of urban areas. In: *Modeling the urban boundary layer*. Boston: American Meteorological Society
- Pielke RA, Martin CL (1981) The derivation of a terrain-following coordinate system for use in a hydrostatic model. *J Atmos Sci* 38: 1707–1731
- Sellers PJ, Mintz Y, Sud YC, Dalcher A (1986) A simple biosphere model (SiB) for use within general circulation models. *J Atmos Sci* 43: 505–531
- Sellers PJ, Hall FG, Asrar G, Strelbel DE, Murphy RE (1992) An overview of the First International Satellite Land Surface Climatology Project (ISLSCP) Field Experiment (FIFE). *J Geophys Res* 97: 18345–18371
- Sellers PJ, Hall FG, Kelly RD, Black A, Baldocchi D, Berry J, Ryan M, Ranson KJ, Crill PM, Lettenmaier DP, Margolis H, Cihlar J, Newcomer J, Fitzjarrald D, Jarvis PG, Gower ST, Halliwell D, Williams D, Goodison B, Wickland DE, Guertin FE (1997) BOREAS in 1997: Experiment overview, scientific results and future directions. *J Geophys Res* 102(D24): 28731–28777
- Thomas G, Rowntree PR (1992) The boreal forests and climate. *Quart J Roy Meteor Soc* 118: 469–497
- Tjernström M (1987) A study of flow over complex terrain using a three-dimensional model. A preliminary model evaluation focusing on stratus and fog. *Annales Geophysicae* 5B: 469–486
- Tjernström M, Enger L, Andrén A (1988) A three-dimensional numerical model for studies of atmospheric flows on the meso- $\gamma$ -scale. *J Theoretical and Appl Mechanics* 7 (Special Issue, Suppl 2): 167–194

- Van den Hurk BJJM, Verhoef A, van den Berg AR, de Bruin HAR (1995) An intercomparison of three vegetation/soil models for a sparse vineyard canopy. *Quart J Roy Meteor Soc* 121: 1867–1889
- Yamada T, Mellor GL (1975) A simulation of the Wangara atmospheric boundary layer data. *J Atmos Sci* 32: 2309–2329

Authors' addresses: Dimitrios Melas, T. Persson, C. Zerefos, Laboratory of Atmospheric Physics, Physics Department, Aristotle University of Thessaloniki, Campus Box 149, GR-54006, Greece; H. DeBruin, Agricultural University Wageningen, The Netherlands; S.-E. Gryning, E. Batchvarova, Wind Energy and Atmospheric Physics Department, Risø National Laboratory, Roskilde, Denmark.